Soliton mode-locking in optical microresonators

T. Herr,[1] V. Brasch,[1] M. L. Gorodetsky,[2,*] and T. J. Kippenberg[1,3,†]

[1] *École Polytechnique Fédérale de Lausanne (EPFL), 1015, Lausanne, Switzerland*
[2] *Faculty of Physics, M.V.Lomonosov Moscow State University, Moscow 119991, Russia*
[3] *Max-Planck-Institut für Quantenoptik, 85748 Garching, Germany*

The discovery of passive mode-locking via saturable absorbers[1, 2] has led to optical femto-second pulses[3, 4] with applications ranging from eye-surgery[5] to the analysis of chemical reactions on ultra-short timescales[6]. In the frequency domain a train of such optical pulses corresponds to a frequency comb (equidistant optical laser lines spaced by the pulse repetition rate)[7–9], which find use in precision spectroscopy and optical frequency metrology[10–12]. Not relying on mode-locking, frequency combs can also be generated in continuously driven, high-quality-factor Kerr-nonlinear optical microresonators via cascaded four-wave mixing[13]. Over the past years these Kerr-combs have been demonstrated in a variety of microresonator geometries [14–20]. Applying a pulse-shaping mode-locking mechanism could enable compact and robust femto-second pulse generators. However, conventional and emerging (e.g. Graphene based) saturable absorbers are challenging to apply to microresonators, as they affect the high-quality-factor essential to nonlinear frequency conversion. Here, we report on passive mode-locking in microresonators without saturable absorber. This mode-locking is achieved via soliton formation[1, 2] supported by the balance between anomalous resonator dispersion and Kerr-nonlinearity induced self-phase modulation. The transitions to and between different soliton states manifest themselves itself as discrete steps in the resonator transmission. Numerical modeling of the nonlinear coupled mode equations is used to physically understand the mode-locking and in combination with an analytical description allows the identification of mode-locked regimes. Experimentally, we observe the generation of pulses with 200 fs duration. Equally important low noise and low line-to-line power variation comb spectra are achieved via single soliton states. These spectra bring microresonator combs decisively closer to frequency domain applications such as channel generators in advanced telecommunication or in fundamental studies such as astrophysical spectrometer calibration[13]. In the time domain the presented results open the route towards compact femto-second sources, where the broadband parametric gain in principle allows for sub-cycle pulses. Moreover, femto-second pulses in conjunction with external broadening provide a viable route to microresonator RF-to-optical links[9, 21].

Frequency comb generation in optical microresonators[22] is achieved via cascaded-four-wave mixing (FWM, cf. Fig 1c) mediated by the Kerr-nonlinearity[14]. Here, a continuous-wave (CW) pump laser is converted into equally spaced optical modes, where the mode spacing corresponds to the free-spectral range (FSR), or equivalently, the inverse resonator roundtrip time $1/T_R$. Driven by a wide range of application in telecommunications[23], spectroscopy[24], astronomy[25, 26], and compact space optical clocks[27] this new class of *Kerr-combs* has rapidly evolved in various materials and geometries[28]. Significant recent advances include the demonstration of octave spanning spectra[29, 30], full phase stabilization[19, 31], low phase noise microwave generation[15, 19, 31, 32], fully planar CMOS compatible design[16, 17, 33], extension of spectral coverage from visible[34] to mid-infrared wavelength[35], as well as arbitrary optical waveform generation[36]. The parametric four-wave mixing process results in coupled phase relations between all the optical modes, which leads to the generation of a periodic time domain output (cf. Fig 1d). Importantly however the output does not correspond intrinsically to pulses. External line-by-line phase and intensity adjustment have been used after comb generation for pulse-shaping[32, 36], but is restricted to a small number of comb modes. Mode-locking, i.e. full phase synchronization *inside* the microresonators would naturally yield a train of optical pulses with a pulse repetition rate $f_{rep} = 1/T_R$ (cf. Fig 1d) and enable ultra-short pulse generation for widespread application. Moreover, mode-locking would provide a way to achieve low-noise frequency comb spectra, with little line-to-line variation and without spectral gaps - a goal difficult to reach in systems with mode-spacings below 100 GHz, where multiple, inconsistent subcombs may form [37].

Introducing a saturable absorber or an equivalent optical element into the laser cavity[1, 2], easily possible in

*Electronic address: michael.gorodetsky@gmail.com
†Electronic address: tobias.kippenberg@epfl.ch

conventional laser systems is hindered by the requirement of a high optical quality factor Q. Still, mode-locking mechanisms intrinsic to microresonators could be present. For instance self-focusing[1, 2], affecting both the intermode coupling inside the resonator as well as the input output coupling to the waveguide. Self-focusing could also induce an intensity dependent surface loss. Moreover, a small saturable component of material absorption could facilitate mode-locking. Interestingly, pump laser detuning dependent transition from high to low phase noise comb states have been observed[20, 30, 37, 38] and interpreted as a signature of potential phase locking [20, 30, 38], but an understanding is still lacking. Analysis of the damped, driven non-linear Schrödinger equation (NLS) suggests that mode-locked regimes could exist in microresonators[39]. It has also been proposed that Kerr-cavity solitons may form in microresonators [40]. This soliton formation could lead to mode-locking[1, 2]. However, to date no definitive proof nor mechanism of mode-locking has been identified.

To reveal potentially mode-locked states as a function of laser detuning we scan the pump laser ω_p (in the direction of decreasing optical frequency) over a high-Q resonance (Q=400 million, free-spectral range FSR=35.2 GHz) of a crystalline MgF_2 resonator[35, 37, 41, 42](cf. Fig. 1a). The radio frequency (RF) signal generated by the beating between neighboring comb lines (down-mixed to 20 MHz) serves as an indicator of mode-locked states. Practically, we sample and subsequently Fourier-transform the RF signal, while the laser scan is performed. In mode-locked states the resulting spectral beat signal is expected to be a single low-noise peak.

Fig. 2b shows the evolution of the optical spectrum during the laser scan. Reducing the laser-cavity detuning leads to a build-up of intra-cavity power and once a critical power threshold is reached widely spaced primary comb modes are generated, followed by secondary modes filling in the spectral gaps as frequently observed (cf. Fig. 1c)[36, 37, 42]. The increase of intra-cavity power also results in a shift of resonance frequency towards lower frequencies via a combined effect of thermal expansion, thermal refractive index change and Kerr-effect. This leads to a non-Lorentzian, triangular resonance shape when the pump laser is tuned with decreasing optical frequency over the resonance (*thermal triangle*, cf. Fig 2a, inset)[43, 44]. Importantly, the thermal effect enables self-locking of the cavity to the laser[44].

The Fourier-transformed, sampled RF signal is contained in Fig. 2c. We observe a transition from a broad, noisy RF signal to a single, low-noise RF beat note. Strikingly, this transition coincides with the beginning of a series of discrete steps in the transmission, which deviate markedly from the expected thermal triangle. Such series of discrete steps have been observed in $\chi^{(2)}$ non-linear microwave resonator, and connected to soliton formation[45]. These observations are highly indicative for mode-locking.

To investigate the intriguing observations of discrete steps in the transmission, and the possible connection to mode-locking we carried out numerical simulations based on the coupled mode-equations approach recently introduced to the field of microresonator combs[46]. The full control over the included physical effects allows identifying the underlying physical mechanisms. Here the simulated system corresponds to a typical MgF_2 microresonator with resonance frequencies $\omega_\mu = \omega_0 + \mu \cdot D_1 + \mu^2 \cdot D_2/2 + \mu^3 \cdot D_3/6$, where $D_1 = 2\pi \cdot FSR$, D_2 and D_3 correspond to the FSR, and the second and third order dispersion around the resonance frequency ω_0 of the pumped mode[37] having the mode index $\mu = 0$. The remaining resonator simulation parameters are refractive and non-linear indices, as well as, the effective mode-volume (cf. methods). We neglect effects of non-unity mode-overlap, interactions with other mode families, any particularities of the resonator geometry and thermal effects. The resulting set of coupled mode equations (cf. methods) is propagated in time using an adaptive step-size Runge-Kutta integrator. Results of a numerical simulation including 101 optical modes are shown in Fig. 3a,b,c. The blue curve in panel a shows the simulated intracavity power as function of $\zeta_o = 2(\omega_0 - \omega_p)/\kappa$, which is a normalized measure of the laser tuning, where $\kappa = \omega_0/Q$ denotes the cavity decay rate. The blue curve is mirrored horizontally for convenience when comparing to the equivalent experimental transmission trace in Fig. 2a (an increased transmission corresponds to a drop in intracavity power). Remarkably, the step features are very well reproduced, implying that the simulation fully includes the relevant physical mechanism. In agreement with the experiment the number and height of steps fluctuate in repeated scans. This last part of comb evolution is sensitive to fluctuations in the pump power and, numerically, short pump power drops can be used to induce a transition to a new comb state. Numerically tracing out all possible comb evolutions yields the orange curves in Fig. 3a. The evolution of the optical spectrum during the scan in Fig. 3a is shown in Fig. 3b and follows the typical path[37]. With each steps the optical spectrum becomes less modulated until it eventually reaches a perfectly smooth envelope state (frame XI).

To reveal mode-locking we investigate the time dependent waveform in Fig. 3c by summing the simulated individual optical modes. Indeed, the first step (frame V) corresponds to a transition to a state where multiple pulses inside the cavity exist. Further steps can be associated with a stepwise reduction of the number of pulses propagating in the resonator. The separation between pulses is random. The presence of anomalous dispersion and Kerr-nonlinearity in the cavity (cf. Fig. 1b) suggests that the pulses may actually be bright, temporal cavity solitons. These have been observed for the first time in a continuously driven fiber-loop cavity and proposed for the case of microresonators frequency combs[40]. To confirm the soliton nature of these pulses we perform a simulation of 501 modes (cf. Fig. 3d,e,f) and analyze a state of five pulses. We compare the numerical simulation with an approximate analytical solution for the damped, driven non-linear Schrödinger (NLS) equation given by a soliton on a CW background [47]

(Note that this NLS equation is equivalent to the coupled mode-equations when neglecting third order dispersion [39]). Based on this, we derive the following expression for multiple solitons

$$\psi(\phi) \simeq \frac{f}{\zeta_0^2} - i\frac{f}{\zeta_0} + \left(\frac{4\zeta_0}{\pi f} + i\sqrt{2\zeta_0 - \frac{16\zeta_0^2}{\pi^2 f^2}}\right)\sum_{j=1}^{N} \mathrm{sech}\left(\sqrt{\frac{\kappa\zeta_0}{D_2}}(\phi - \phi_j)\right), \tag{1}$$

where ψ denotes the complex field amplitude, ϕ the angular coordinate inside the resonator, ϕ_j the angular coordinate of the jth soliton, ω_p the pump power, N is the number of solitons, and f corresponds to the pump power (cf. methods). We note that this solution, except for the soliton positions ϕ_i, does not include any free parameters. Indeed, the close to perfect match between analytical solution and numerical result shows, that the pulses forming in the microresonator are temporal cavity solitons. Eq. 1 allows to estimate the detuning and dispersion dependent temporal width of the soliton $T_s = \sqrt{D_2/2\zeta_0}/D_1$. Note that due to the non-linear Kerr-shift of the resonance frequency, the effective detuning between pump laser and resonance is smaller than ζ_0.

Having revealed the soliton nature of the pulses in numerical simulation, we can interpret the blue curve in Fig. 3a based on general limits applying to solitons as solutions of the driven, damped NLS[48]. Adopting these criteria for the present case we identify three main regions colored red, yellow and green in Fig. 3a. Solitons with a constant temporal envelope can only exist in the green area. While the yellow area still allows for solitons with time varying envelope (breather solitons) [49], solitons can not exist in the red area. The curves defining the yellow area are given by $\overline{|a|^2}_{\pm} = \frac{2}{3}\zeta_0 \pm \frac{1}{3}\sqrt{\zeta_0^2 - 3}$, where $\overline{|a|^2}$ refers to the average energy in the resonator. An additional restriction limits detuning to $\zeta_0 = \pi^2/8f^2$, beyond which no solitons can exist[48]. Note that in the red area on the left the system may undergo chaotic Hopf-bifurcations[48]. The correspondence of these analytical limits with the numerical results is remarkable.

By averaging the analytical soliton solution (eq. 1), for different number of solitons, over one cavity roundtrip time we can derive the total internal field inside the resonator. The result is shown as dark gray dashed lines, which are in excellent agreement with the numerically observed steps (to account for the limitation due to the low mode number an additional correction factor of order unity is applied). The step height is directly proportional to the number of solitons removed in a comb transition.

The simulations show that microresonators can intrinsically be mode-locked via soliton-formation[1, 2], which relies on the anomalous cavity dispersion and the Kerr-non-linearity causing frequency and intensity dependent phase shifts. Other physical mechanism, particularly an additional saturable absorber, are not included in the simulation. For completeness we note that the soliton transition may also be observed in simulations of an injection locked operation scheme, where the pump power is gradually increased and the laser remains at zero detuning with respect to the non-linearly shifted resonance.

Having reached a theoretical understanding of the soliton states, we next experimentally investigate - in addition to their RF beatnote and optical spectrum - their temporal characteristics by performing a frequency-resolved optical gating experiment (FROG, Fig. 4a and 4e for the setup)[50]. This corresponds to a second-harmonic generation (SHG) autocorrelation experiment, where the frequency-doubled light is spectrally resolved (cf. methods). In full consistency with the numerical simulations, we observe single and multiple pulse states as shown in Fig. 3c. The one pulse state is characterized by a smooth spectral envelope, without spectral gaps. The power spectral envelope exhibits a squared hyperbolic secant sech^2-shape (with FWHM = 1.6 THz) as expected from the Fourier transform of a sech-shaped soliton pulse. Based on the time-bandwidth-product of 0.315 the expected pulse duration is 197 fs. The low phase noise RF beatnote is resolution bandwidth limited to 1 kHz and its signal-to-noise ratio exceeds 60 dB. The FROG trace shows pulses well separated by the cavity roundtrip time of T_R =28.4 ps, corresponding to the FSR of 35.2 GHz. The multi-pulse states (here shown for the case of two and five pulses), show a more structured optical spectrum. This structure reflects the number and distribution of pulses in the cavity. The RF beat note generated in the multi-pulse states is of similar quality as in the single pulse state. Importantly, the FROG measurement allows for a full reconstruction (neglecting a time direction ambiguity) of intensity and phase of the pulses (cf. Fig. 4b). The reconstructed intensity is consistent with the expected sech^2-shape for solitons and has a FWHM of 200 fs in agreement with the expectation. The FROG traces show that it is the full optical spectrum that contributes to the pulses. This is particularly true in the case of multiple pulses.

Combining experimental, numerical and analytical results, we have demonstrated mode-locking in a MgF_2 microresonator via soliton formation, which is only based on the generic properties of Kerr nonlinear microresonators with anomalous dispersion. Consequently, our observations are generic and apply equally to other Kerr comb platforms. From a frequency domain perspective, soliton mode-locking enables microresonator based frequency combs with low noise and smooth spectral envelope. Such low line-to-line variations are key to applications such as channel generation for advanced modulation formats in telecommunication. From a time domain perspective it enables ultra-short soliton pulse generation in a microresonator. In combination with chip-scale[16, 17] integration this opens the route towards

compact, low cost ultra-short pulsed lasers sources . Due to the broadband nature of the parametric gain, which can significantly exceed the spectral width of conventional laser gain media, the direct synthesis of sub-cycle pulses with this method is conceivable.

I. METHODS

Kerr-Comb generation: The pump laser used is a narrow linewidth (100 kHz shortterm) 1553 nm fiber laser amplified by an erbium doped fiber amplifer (EDFA). Evanescent coupling of the resonator is achieved via a tapered optical fiber[51] yielding a coupled linewidth of $\kappa/2\pi = 450$ kHz.

Numerical simulation: Besides the resonance frequencies ω_μ defined by $D_1/2\pi = 35.2$ GHz, $D_2/2\pi = 10$ kHz, $D_3/2\pi = -130$ Hz as measured[52], the resonator is characterized by its refractive and non-linear Kerr indices $n = 1.37$ and $n_2 = 0.9 \times 10^{-20}$ m^{2}W^{-1}, the effective mode volume[53] $V_{eff} = 5.6 \times 10^{-13}$ m^3 and quality factor $Q = 250 \times 10^6$. Starting from the coupled mode equations for the non-equidistant cavity modes A_μ at the resonance freqeuncies ω_μ a set of dimensionless coupled mode equations for the equidistant comb modes a_μ at a priori unknown frequencies can be derived (cf. SI in [37]). The mode amplitudes are related via the transformation $a_\mu = A_\mu \sqrt{2g/\kappa} e^{i(\omega_\mu - \omega_p - \mu D_1)t}$ where $|A_\mu|^2$ is the number of photons. The coupled mode equations read:

$$\frac{\partial a_\mu}{\partial \tau} = -[1 + i\zeta_\mu]a_\mu + i \sum_{\mu'=-K}^{K} \sum_{\mu'' \geq \mu'} (2 - \delta_{\mu'\mu''}) a_{\mu'} a_{\mu''} a^*_{\mu'+\mu''-\mu} + \delta_{0\mu} f. \tag{2}$$

The Kerr non-linearity is contained in the nonlinear coupling coefficient $g = \frac{\hbar\omega_0^2 c n_2}{n^2 V_{eff}}$, $f = \sqrt{\frac{8gP_{in}}{\kappa\hbar\omega_0}}$ is the normalized driving field, and $\tau = \kappa t/2$ the cavity intrinsic time scale. $2K + 1$ is the number of simulated modes and $\zeta_\mu = 2(\omega_\mu - \omega_p - \mu D_1)/\kappa$. In a post-processing step the optical frequencies, field amplitudes, phases and RF signal can be inferred by taking amplitude and phase modulation of the simulated field amplitudes a_μ into account. Random vacuum fluctuations are used to seed initial FWM. The pump power is set to $P_{\rm in} = 100$mW at a pump frequency of $\omega_p = 193$ THz. The computation time scales cubically to highest order and a simulation of 501 modes takes 5 days on a standard PC.

FROG Experiment: Prior to the FROG experiment[50] the optical spectra are sent through a fiber-Bragg grating for pump supression (30 dB) and subsequently amplified to 50 mW. Dispersion compensating fiber (DCF3,DCF38) is used for approximate dispersion compensation. In the FROG setup (cf. Fig 4c) the generated optical pulses, are interferometrically split and recombined with an adjustable delay in a non-linear crystal resulting in self-gated second harmonic generation (SHG), that is doubling of the optical frequency whenever the optical pulses in the two arms of the interferometer overlap temporally in the non-linear BBO crystal. The generated SHG light is spectrally resolved and recorded as a function of delay, yielding a so called FROG trace. Each scan consist of nearly 1000 spectra with individual exposure times of 800 ms. The higher resolution N-by-N (N=63) FROG trace of the single pulse state in Fig. 4b) is analyzed using a principal component generalized projection FROG algorithm, after noise removal via Fourier-filtering. The FROG reconstruction error is defined as $\epsilon = \frac{1}{N}\sqrt{\sum_{i,j}^{N}(M_{ij}^{meas} - M_{ij}^{reco})^2}$, where M_{ij}^{meas} and M_{ij}^{reco} denote the elements of the $N \times N$ matrices representing the measured and reconstructed FROG traces.

II. ACKNOWLEDGEMETS

This work was supported by the DARPA program QuASAR, the Swiss National Science Foundation (SFN) as well as a Marie Curie IAPP program. MLG acknowledges support from the "Dynasty" foundation and RFBR grant 11-02-00383-a

[1] H. A. Haus. Mode-locking of lasers. *Ieee Journal of Selected Topics In Quantum Electronics*, 6(6):1173–1185, November 2000.

[2] U. Keller. Recent developments in compact ultrafast lasers. *Nature*, 424(6950):831–838, 2003.

[3] E. Ippen and C. Shank. Sub-picosecond, kilowatt pulses from a mode-locked CW dye laser. *IEEE Journal of Quantum Electronics*, 10:722–722, September 1974. doi: 10.1109/JQE.1974.1068270.

[4] G. Steinmeyer, D. H. Sutter, L. Gallmann, N. Matuschek, and U. Keller. Frontiers in ultrashort pulse generation: Pushing the limits in linear and nonlinear optics. *Science*, 286(5444):1507–1512, 1999. doi: 10.1126/science.286.5444.1507.

[5] F. H. Loesel, R. M. Kurtz, C. Horvath, S. I. Sayegh, G. A. Mourou, J. F. Bille, and T. Juhasz. Ultraprecise medical applications with ultrafast lasers: corneal surgery with femtosecond lasers. In G. B. Altshuler, S. Andersson-Engels, R. Birngruber, P. Bjerring, A. F. Fercher, H. J. Geschwind, R. Hibst, H. Hoenigsmann, F. Laffitte, and H. J. Sterenborg, editors, *Society of Photo-Optical Instrumentation Engineers (SPIE) Conference Series*, volume 3564 of *Society of Photo-Optical Instrumentation Engineers (SPIE) Conference Series*, pages 86–93, February 1999.

[6] A. H. Zewail. Laser Femtochemistry. *Science*, 242:1645–1653, December 1988. doi: 10.1126/science.242.4886.1645.

[7] R. Holzwarth, T. Udem, T. W. Hansch, J. C. Knight, W. J. Wadsworth, and P. S. J. Russell. Optical frequency synthesizer for precision spectroscopy. *Physical Review Letters*, 85:2264–2267, 2000.

[8] D. J. Jones, S. A. Diddams, J. K. Ranka, A. Stentz, R. S. Windeler, J. L. Hall, and S. T. Cundiff. Carrier-envelope phase control of femtosecond mode-locked lasers and direct optical frequency synthesis. *Science*, 288:635–639, 2000.

[9] S. T. Cundiff and J. Ye. Colloquium: Femtosecond optical frequency combs. *Reviews of Modern Physics*, 75(1):325, 2003.

[10] Th. Udem, R. Holzwarth, and T. W. Hänsch. Optical frequency metrology. *Nature*, 416:233–237, 2002.

[11] N. R. Newbury. Searching for applications with a fine-tooth comb. *Nature Photonics*, 5:186–188, 2011.

[12] R. van Rooij, J. S. Borbely, J. Simonet, M. D. Hoogerland, K. S. E. Eikema, R. A. Rozendaal, and W. Vassen. Frequency Metrology in Quantum Degenerate Helium: Direct Measurement of the $2\ ^3S_1 \rightarrow 2\ ^1S_0$ Transition. *Science*, 333:196–, July 2011. doi: 10.1126/science.1205163.

[13] T. J. Kippenberg, R. Holzwarth, and S. A. Diddams. Microresonator-based optical frequency combs. *Science*, 332:555, 2011.

[14] P. Del'Haye, A. Schliesser, O. Arcizet, T. Wilken, R. Holzwarth, and T. Kippenberg. Optical frequency comb generation from a monolithic microresonator. *Nature*, 450:1214–1217, 2007.

[15] A. A. Savchenkov, A. B. Matsko, V. S. Ilchenko, I. Solomatine, D. Seidel, and L. Maleki. Tunable optical frequency comb with a crystalline whispering gallery mode resonator. *Physical Review Letters*, 101:093902, 2008.

[16] J. S. Levy, A. Gondarenko, M. A. Foster, A. C. Turner-Foster, A. L. Gaeta, and M. Lipson. Cmos-compatible multiple-wavelength oscillator for on-chip optical interconnects. *Nature Photonics*, 4(1):37–40, January 2010.

[17] L. Razzari, D. Duchesne, M. Ferrera, R. Morandotti, S. Chu, B. E. Little, and D. J. Moss. Cmos-compatible integrated optical hyper-parametric oscillator. *Nature Photonics*, 4(1):41–45, January 2010.

[18] A. A. Savchenkov, A. B. Matsko, W. Liang, V. S. Ilchenko, D. Seidel, and L. Maleki. Kerr combs with selectable central frequency. *Nature Photonics*, 5:293–296, May 2011. doi: 10.1038/nphoton.2011.50.

[19] S. B. Papp, P. Del'Haye, and S. A. Diddams. Mechanical control of a microrod-resonator optical frequency comb. *ArXiv e-prints*, May 2012.

[20] J. Li, H. Lee, T. Chen, and K. J. Vahala. Low-Pump-Power, Low-Phase-Noise, and Microwave to Millimeter-wave Repetition Rate Operation in Microcombs. *ArXiv e-prints*, August 2012.

[21] H. R. Telle, G. Steinmeyer, A. E. Dunlop, J. Stenger, D. H. Sutter, and U. Keller. Carrier-envelope offset phase control: A novel concept for absolute optical frequency measurement and ultrashort pulse generation. *Applied Physics B-Lasers And Optics*, 69(4):327–332, October 1999.

[22] K. J. Vahala. Optical microcavities. *Nature*, 424(6950):839–846, 2003.

[23] Joerg Pfeifle, Claudius Weimann, Florian Bach, Johann Riemensberger, Klaus Hartinger, David Hillerkuss, Meinert Jordan, Ronald Holtzwarth, Tobias J. Kippenberg, Juerg Leuthold, Wolfgang Freude, and Christian Koos. Microresonator-based optical frequency combs for high-bitrate wdm data transmission. In *Optical Fiber Communication Conference*, page OW1C.4. Optical Society of America, 2012.

[24] S. A. Diddams, L. Hollberg, and V. Mbele. Molecular fingerprinting with the resolved modes of a femtosecond laser frequency comb. *Nature*, 445:627–630, 2007.

[25] T. Steinmetz, T. Wilken, C. Araujo-Hauck, R. Holzwarth, T. W. Hänsch, L. Pasquini, A. Manescau, S. D'Odorico, M. T. Murphy, T. Kenitscher, W. Schmidt, and T. Udem. Laser frequency combs for astronomical observations. *Science*, 321: 1335–1337, 2008.

[26] C.-H. Li, A. J. Benedick, P. Fendel, A. G. Glenday, F. X. Kärtner, D. F. Philips, D. Sasselov, A. Szentgyorgyi, and R. L. Walsworth. A laser frequency comb that enables radial velocity measurements with a precision of 1 cm s^{-1}. *Nature*, 452: 610–612, 2008.

[27] S. Schiller, A. Görlitz, A. Nevsky, S. Alighanbari, S. Vasilyev, C. Abou-Jaoudeh, G. Mura, T. Franzen, U. Sterr, S. Falke, C. Lisdat, E. Rasel, A. Kulosa, S. Bize, J. Lodewyck, G. M. Tino, N. Poli, M. Schioppo, K. Bongs, Y. Singh, P. Gill, G. Barwood, Y. Ovchinnikov, J. Stuhler, W. Kaenders, C. Braxmaier, R. Holzwarth, A. Donati, S. Lecomte, D. Calonico, and F. Levi. The Space Optical Clocks Project: Development of high-performance transportable and breadboard optical clocks and advanced subsystems. *ArXiv e-prints*, June 2012.

[28] T. Kippenberg, P. Del'Haye, and A. Schliesser. Method and apparatus for optical frequency comb gneration using a monolithic microresonator, Jul 2011.

[29] P. Del'Haye, T. Herr, E. Gavartin, M. L. Gorodetsky, R. Holzwarth, and T. J. Kippenberg. Octave spanning tunable frequency comb from a microresonator. *Phys. Rev. Lett.*, 107(6):063901, Aug 2011. doi: 10.1103/PhysRevLett.107.063901.

[30] Y. Okawachi, K. Saha, J. S. Levy, Y. H. Wen, M. Lipson, and A. L. Gaeta. Octave-spanning frequency comb generation in a silicon nitride chip. *Opt. Lett.*, 36(17):3398–3400, Sep 2011. doi: 10.1364/OL.36.003398.

[31] P. Del'Haye, O. Arcizet, A. Schliesser, R. Holzwarth, and T. J. Kippenberg. Full stabilization of a microresonator-based optical frequency comb. *Physical Review Letters*, 101:053903, 2008.

[32] Scott B. Papp and Scott A. Diddams. Spectral and temporal characterization of a fused-quartz-microresonator optical frequency comb. *Phys. Rev. A*, 84:053833, Nov 2011. doi: 10.1103/PhysRevA.84.053833.

[33] M. A. Foster, J. S. Levy, O. Kuzucu, K. Saha, M. Lipson, and A. L. Gaeta. Silicon-based monolithic optical frequency comb source. *Opt. Express*, 19(15):14233–14239, Jul 2011. doi: 10.1364/OE.19.014233.

[34] A. A. Savchenkov, A. B. Matsko, W. Liang, V. S. Ilchenko, D. Seidel, and L. Maleki. Kerr combs with selectable central frequency. *Nature Photonics*, 5:293–296, May 2011. doi: 10.1038/nphoton.2011.50.

[35] C. Y. Wang, T. Herr, P. Del'Haye, A. Schliesser, J. Hofer, R. Holzwarth, T. W. Hänsch, N. Picque, and T. J. Kippenberg. Mid-infrared optical frequency combs based on crystalline microresonators. *arXiv:1109.2716*, 2011.

[36] F. Ferdous, H. Miao, D. E. Leaird, K. Srinivasan, J. Wang, L. Chen, L. T. Varghese, and A. M. Weiner. Spectral line-by-line pulse shaping of on-chip microresonator frequency combs. *Nature Photonics*, 5:770–776, December 2011. doi: 10.1038/nphoton.2011.255.

[37] T. Herr, K. Hartinger, J. Riemensberger, C. Y. Wang, E. Gavartin, R. Holzwarth, M. L. Gorodetsky, and T. J. Kippenberg. Universal formation dynamics and noise of Kerr-frequency combs in microresonators. *Nature Photonics*, 6:480–487, July 2012. doi: 10.1038/nphoton.2012.127.

[38] Adrea R. Johnson, Yoshitomo Okawachi, Jacob S. Levy, Jaime Cardenas, Kasturi Saha, Michal Lipson, and Alexander L. Gaeta. Chip-based frequency combs with sub-100ghz repetition rates. *Opt. Lett.*, 37(5):875–877, Mar 2012. doi: 10.1364/OL.37.000875.

[39] A. B. Matsko, A. A. Savchenko, W. Liang, V. S. Ilchenkko, D. Seidel, and L. Maleki. Mode-locked kerr frequency combs. *Optics Letters*, 36:2845–2847, 2011.

[40] F. Leo, S. Coen, P. Kockaert, S. P. Gorza, P. Emplit, and M. Haelterman. Temporal cavity solitons in one-dimensional kerr media as bits in an all-optical buffer. *Nature Photonics*, 4(7):471–476, July 2010.

[41] W. Liang, A. A. Savchenkov, A. B. Matsko, V. S. Ilchenko, D. Seidel, and L. Maleki. Generation of near-infrared frequency combs from a mgf2 whispering gallery mode resonator. *Opt. Lett.*, 36(12):2290–2292, Jun 2011. doi: 10.1364/OL.36.002290.

[42] Ivan S. Grudinin, Lukas Baumgartel, and Nan Yu. Frequency comb from a microresonator with engineered spectrum. *Opt. Express*, 20(6):6604–6609, Mar 2012. doi: 10.1364/OE.20.006604.

[43] M. L. Gorodetsky and V. S. Ilchenko. Thermal nonlinear effects in optical whispering-gallery microresonators. *Laser Physics*, 2:1004–1009, 1992.

[44] T. Carmon, L. Yang, and K. J. Vahala. Dynamical thermal behavior and thermal selfstability of microcavities. *Optics Express*, 12:4742–4750, 2004.

[45] A. Gasch, B. Wedding, and D. Jäger. Multistability and soliton modes in nonlinear microwave resonators. *Applied Physics Letters*, 44:1105–1107, June 1984. doi: 10.1063/1.94658.

[46] Y. K. Chembo and N. Yu. Modal expansion approach to optical-frequency-comb generation with monolithic whispering-gallery-mode resonators. *Physical Reveiw A*, 82(3):033801, Sep 2010. doi: 10.1103/PhysRevA.82.033801.

[47] S. Wabnitz. Suppression of soliton interactions by phase modulation. *Electronics Letters*, 29(19):1711 –1713, sept. 1993. ISSN 0013-5194. doi: 10.1049/el:19931138.

[48] I. V. Barashenkov and Yu. S. Smirnov. Existence and stability chart for the ac-driven, damped nonlinear schrödinger solitons. *Phys. Rev. E*, 54:5707–5725, Nov 1996. doi: 10.1103/PhysRevE.54.5707.

[49] A. Matsko, A. Savchenko, and L. Maleki. On excitation of breather solitons in an optical microresonator. *Optics Letters (early posting)*, 2012.

[50] Daniel J. Kane. Principal components generalized projections: a review. *J. Opt. Soc. Am. B*, 25(6):A120–A132, Jun 2008. doi: 10.1364/JOSAB.25.00A120.

[51] S. M. Spillane, T. J. Kippenberg, O. J. Painter, and K. J. Vahala. Ideality in a fiber-taper-coupled microresonator system for application to cavity quantum electrodynamics. *Physical Review Letters*, 91(4):043902, 2003.

[52] P Del'Haye, O. Arciezt, M. L. Gorodetsky, R. Holzwarth, and T. J. Kippenberg. Frequency comb assisted diode laser spectroscopy for measurement of microcavity dispersion. *Nature Photonics*, pages 529–533, 2009.

[53] M. L. Gorodetsky and Yu. A. Demchenko. Accurate analytical estimates of eigenfrequencies and dispersion in whispering-gallery spheroidal resonators. In A. V. Kudryashov, Paxton A. H., and V. S. Ilchenko, editors, *Laser Resonators, Microresonators, and Beam Control XIV*, volume 8236 of *Proceedings of SPIE*, 2009. ISBN 9780819488794. doi: 10.1117/12.914606.

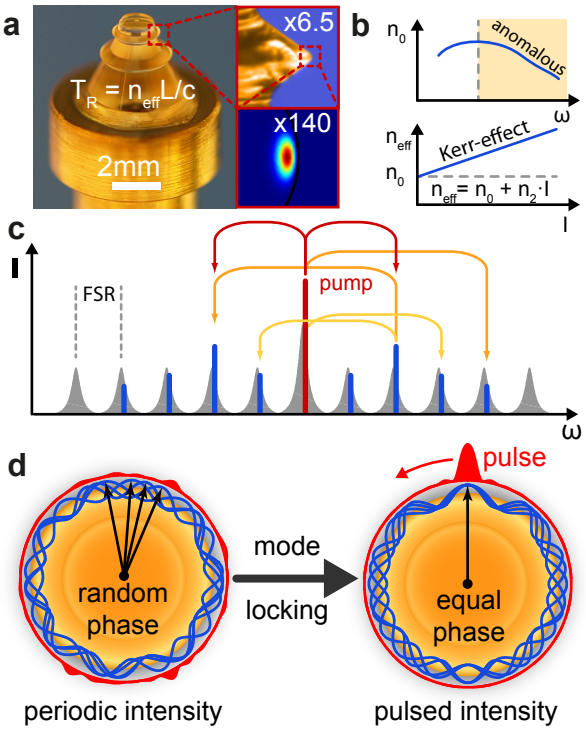

FIG. 1: **Fig.1 Mode-locking and frequency comb generation in microresonators.** **a.** MgF_2 crystal carrying two whispering-gallery-mode microresonator of different size (here: the smaller one with an FSR of 35.2 GHz is used). Here an optical whispering-gallery-mode propagates along the circumference L of the resonator within the roundtrip time T_R. The magnified panels show a zoom in and the simulated optical mode profile. **b.** Anomalous dispersion and Kerr-effect leading to a frequency ω dependent and intensity I dependent effective refractive index n_{eff} (n_0: refractive index; n_2: nonlinear refractive index). **c.** Frequency comb generation in Kerr-nonlinear microresonator via four-wave-mixing, The newly generated optical lines are supported by the cavity's resonances (gray). Widely spaced primary lines emerge first, followed by secondary comb lines filling the gaps. **d.** Optical whispering gallery comb modes (blue) and resulting intensity (red). If the relative phases (indicated by the black arrows) are constant but random the resulting intensity is periodic with T_R; if the phases are synchronized via mode-locking the resulting intensity is pulsed with a pulse repetition rate of $1/T_R$.

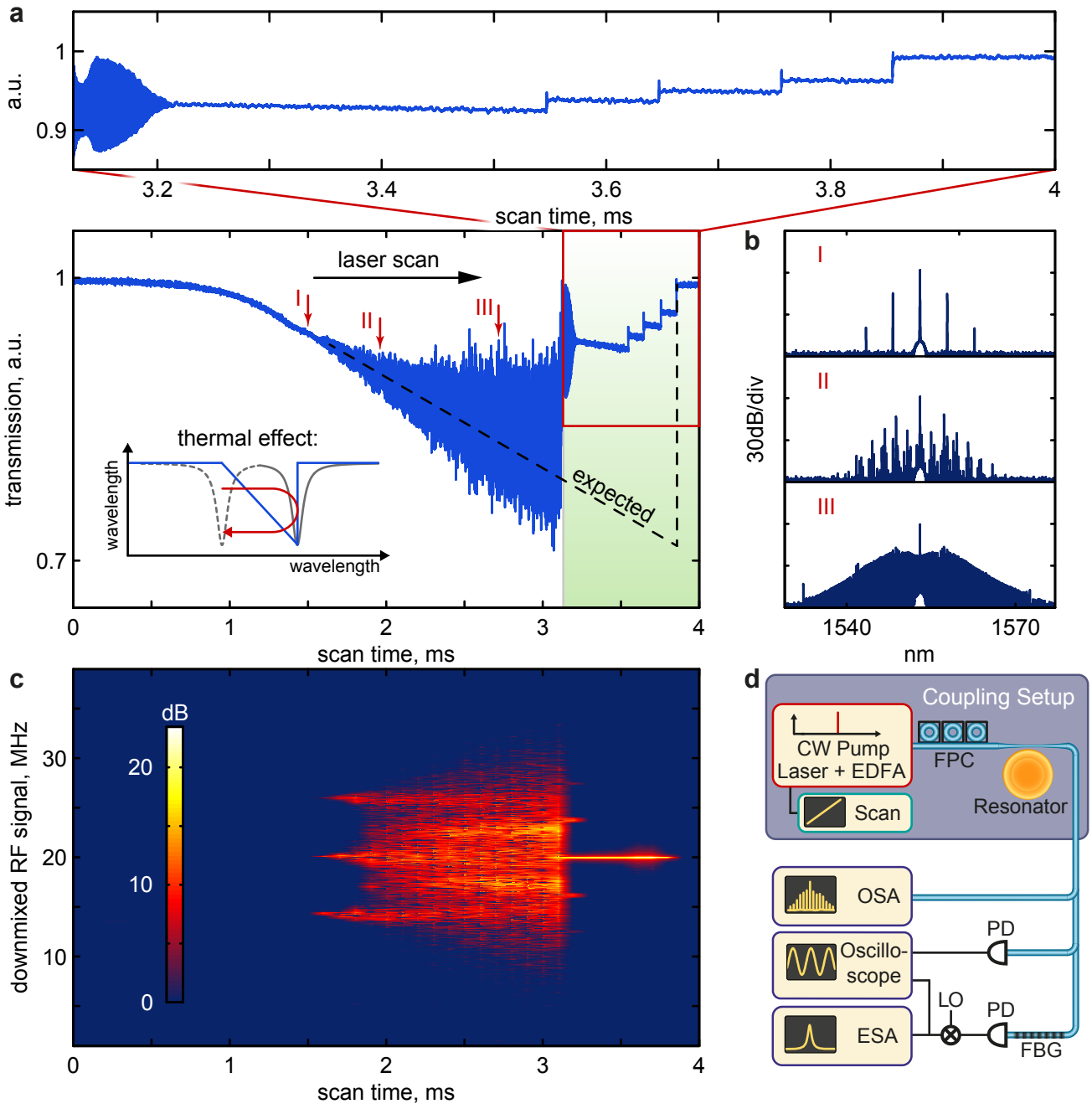

FIG. 2: **Fig.2 Transmission and beatnote a.** Transmission observed when scanning a laser over a high-Q Kerr-non-linear resonance in a MgF_2 resonator (coupled pump power 5 mW). The transmission signal follows the expected thermal triangle (cf. inset) with deviations in the form of discrete steps (green shading). **b.** Evolution of the optical spectrum for three different positions in the scan (I,II,III). **c.** Downmixed radio frequency (RF) beat signal. **d.** Experimental setup composed of generic coupling setup (including pump laser and resonator) followed by an optical spectrum analyzer (OSA), an oscilloscope to record the transmission and to sample the down-mixed beatnote (via the third harmonic of a local oscillator LO at 11.7 GHz), and an electrical spectrum analyzer (ESA) to monitor the beatnote. Before beatnote detection the pump is filtered out by a narrow fiber-Bragg grating (FBG) in transmission (FPC: Fiber polarization controller; CW continuous wave; EDFA: erbium-doped fiber amplifier; PD: photodiode).

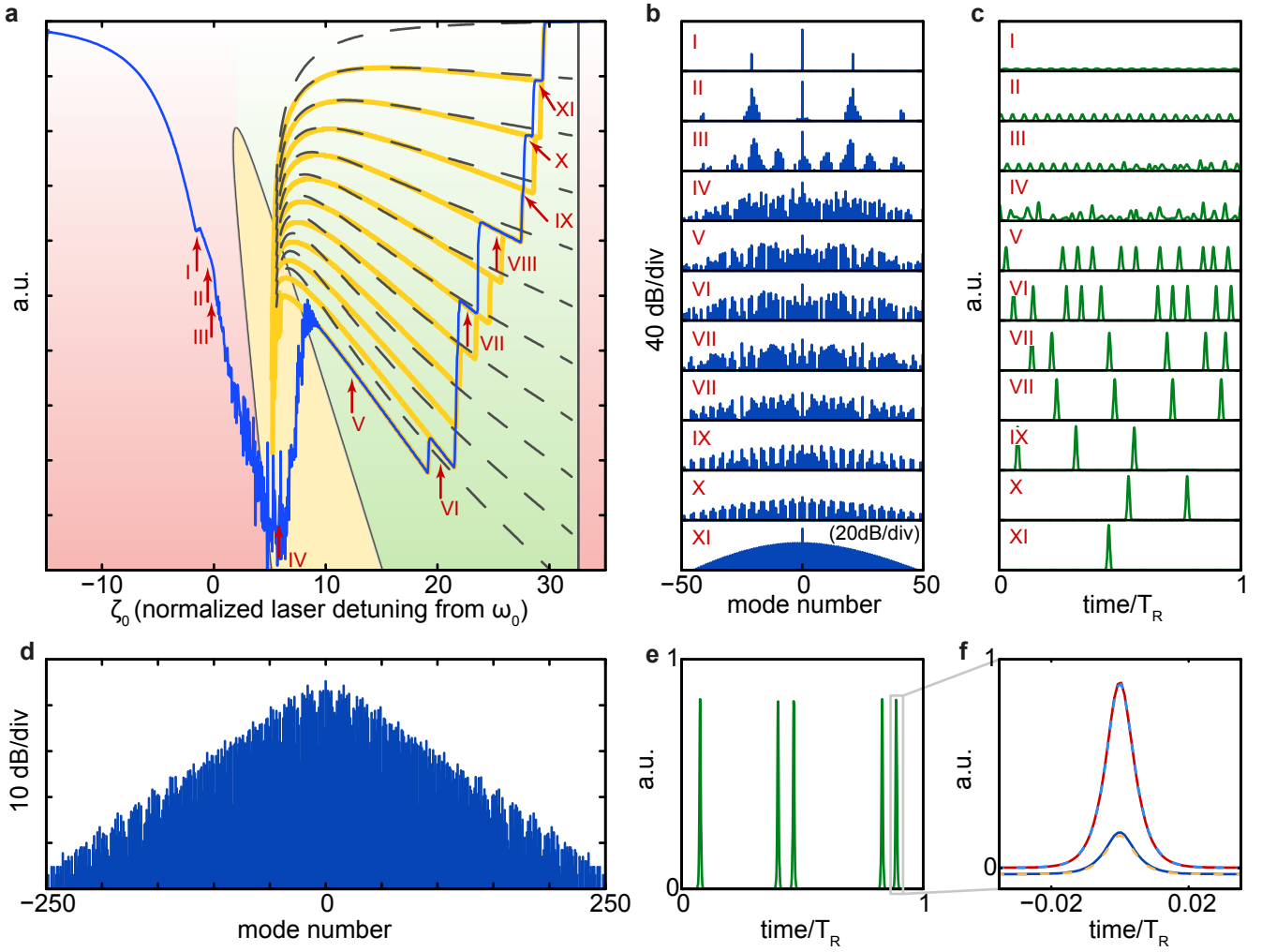

FIG. 3: **Fig.3 Numerical Simulations a.** Transmission (blue) in a simulated laser scan over a resonance in a MgF_2 resonator leading to step-like features (101 simulated modes). The orange lines trace out all possible transmission evolutions of the system. The dashed lines show an analytical description of the steps. The green area corresponds to the area, where solitons can exist, the yellow area allows for solitons with time variable envelope; no solitons can exist in the red area. **b/c.** Optical spectrum and intracavity intensity for different positions I-XI in the laser scan. **d.** Optical spectrum obtained when simulating 501 modes and stopping the laser scan in the soliton-regime. **e.** Intracavity intensity for the comb state in (d) showing 5 solitons. **f.** Zoom into one of the soliton states showing the numerical results for the field real (red) and imaginary part (dark blue). The respective analytical soliton solutions are shown in dashed light blue and orange.

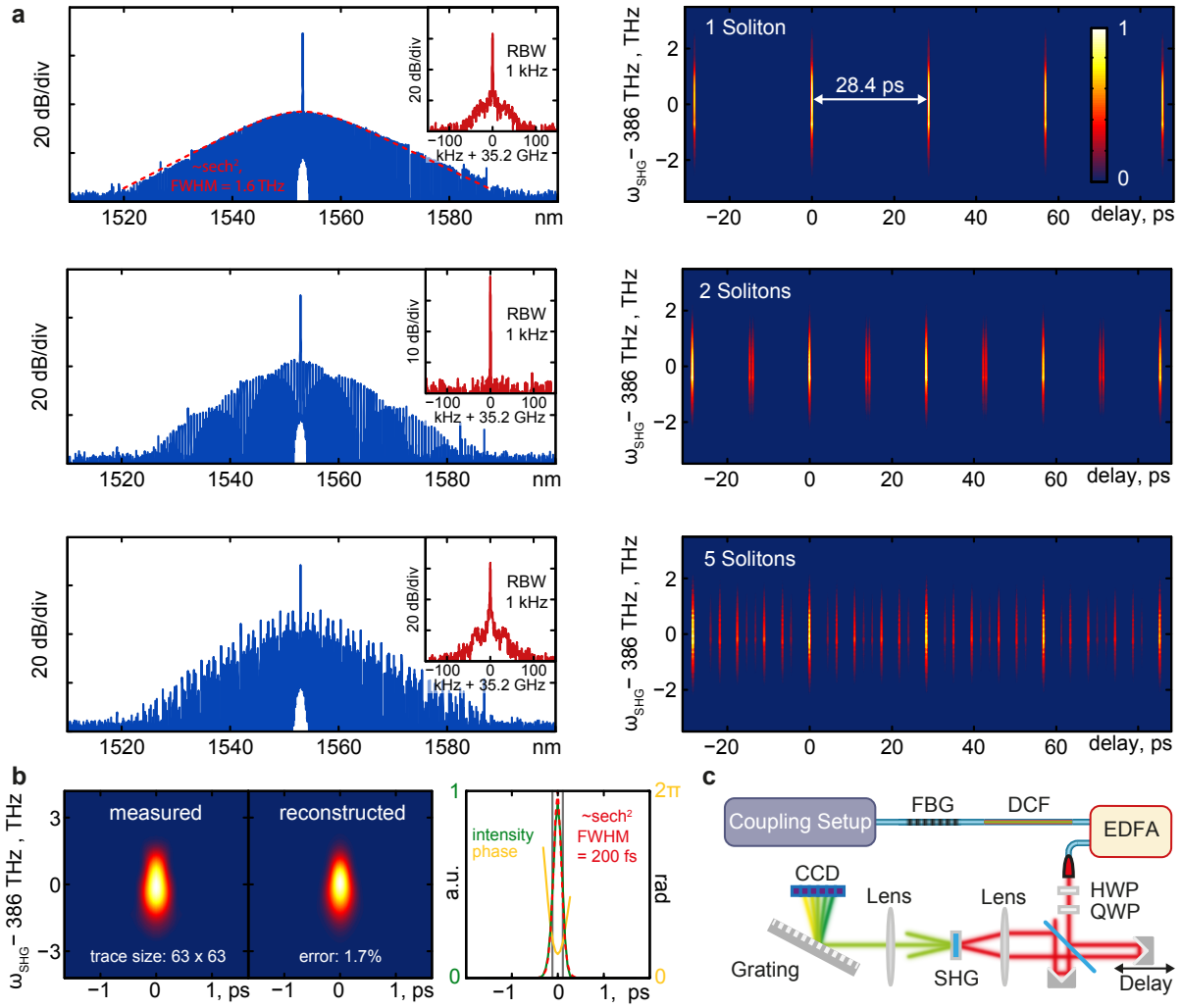

FIG. 4: **Fig.4 Experimental demonstration of soliton states a.** Optical spectra (left column) of three select comb states (one, two and five pulses). The insets show the RF beat note, which is resolution bandwidth limited to 1 kHz width in all cases. The FROG (frequency resolved optical gating) traces (right column) reveal single and multiple pulses per cavity roundtrip time. The red line in the optical spectrum of the one pulse state shows the spectral hyperbolic-secant envelope expected for soliton pulses with a full-width-half-maximum (FWHM) of 1.6 THz. **b.** Higher resolution experimental FROG trace of a one soliton pulse (left). The reconstruction converges to a FROG error of 1.7% in good agreement (middle) with the experimental trace. The reconstruction yields an estimated pulse duration of 200 fs (FWHM). **c.** Setup for the FROG experiment: After pulse generation in the microresonator (cf. Coupling Setup, Fig. 2) the pump light is filtered out using a fiber-Bragg grating (FBG) in transmission. The optical signal is dispersion compensated via dispersion compensating fiber (DCF3, DCF38) and amplified in an erbium doped fiber amplifier (EDFA) to approx. 50 mW. The amplified light is free-space coupled to an Michelson-type interferometer with offset beams. Focused by a lens the two beams overlap in a non-linear BBO crystal for frequency doubling. Only the frequency doubled beam in the central forward direction is allowed to reach a grating based CCD-spectrometer for detection. The delay of the interferometer is varied to record the frequency doubled optical signal spectrally resolved as a function of delay (HWP: half-wave-plate, QWP: quarter-wave-plate).